The Meteoritical Society

Meteoritics & Planetary Science 46, Nr 4, 534–542 (2011)
doi: 10.1111/j.1945-5100.2011.01172.x

Photometric observations of Earth-impacting asteroid 2008 TC_3

Marek J. KOZUBAL[1*], Forrest W. GASDIA[1], Ronald F. DANTOWITZ[1], Peter SCHEIRICH[2], and Alan W. HARRIS[3]

[1]Clay Center Observatory, Dexter and Southfield Schools, 20 Newton St., Brookline, Massachusetts 02445, USA
[2]Astronomical Institute, Academy of Sciences of the Czech Republic, Fričova 1, 25165 Ondřejov, Czech Republic
[3]Space Science Institute, 4603 Orange Knoll Ave., La Canada, California 91011–3364, USA
[*]Corresponding author. E-mail: mkozubal@dexter.org

(Received 26 March 2010; revision accepted 16 December 2010)

Abstract–A calibrated lightcurve is presented of the near-Earth asteroid 2008 TC_3, obtained before it impacted Earth on October 7, 2008. The asteroid was observed in unfiltered images from the end of astronomical twilight until the object entered Earth's shadow about 2 h later. The observations covered a wide range of phase angles from 14.79° to 2.93°, during which the asteroid ranged from 82,000 km to 29,000 km distance from the observer. A method is presented for obtaining photometrically filtered brightness values for the asteroid using unfiltered imaging techniques. Over 1,700 images of the asteroid produce a lightcurve with a peak-to-peak variation in V of 0.76 magnitude. Analysis of the lightcurve yields values for $H = 30.86 \pm 0.01$ and $G = 0.33 \pm 0.03$. Combined with other constraints on the kinetic energy and diameter of the asteroid, which suggest a low 1.8 g cm^{-3} density and albedo 0.05 ± 0.01, the value of H implies an asteroid of about 4.1 m in diameter, 28 m^3 in volume, and 51,000 kg in mass. The determined value of G is out of range for normal, larger asteroids of albedo 0.05–0.15.

INTRODUCTION

The Catalina Sky Survey discovered the near-Earth asteroid 2008 TC_3 at 6:39 UT on October 6, 2008 (Kowalski et al. 2008). The Minor Planet Center soon after suggested an atmospheric entry within 21 h of its discovery. The Jet Propulsion Laboratory later predicted an entry over Sudan at about 2:46 UT on October 7 (Chesley et al. 2008; Yeomans 2008). Notifications were sent out via the Minor Planet Center mailing list. Kenyan infrasonic sensors and United States government satellites both detected the object's atmospheric entry over the Sudanese desert (Chesley et al. 2008). Predictions were that the asteroid would not survive atmospheric entry; however, it was possible that meteorite fragments would make it to the ground. In December, several pieces were recovered in the Nubian Desert and were named Almahata Sitta (Jenniskens et al. 2009). This was the first near-Earth object detected before hitting Earth's atmosphere, and the first asteroid observed before being recovered in the form of meteorites.

The size of the asteroid and quantity of energy released during the impact is important for understanding how unusual this detection was, what the initial conditions before impact were, and how much material did survive in the form of meteorites. The size of the asteroid was derived from the reported absolute brightness, H, in magnitude (Jenniskens et al. 2009). This absolute magnitude relates to the size of the object, via the albedo, for which values adopted were derived from the recovered meteorites. The value for G relates to the asteroid's physical surface light scattering properties because it describes the importance of the opposition effect (enhanced backscattering of light).

A size of between 3 and 4 m was derived from our preliminary value of $H = 30.9 \pm 0.1$ magnitude, for an assumed slope parameter of $G = 0.15$.

To improve this estimate, the asteroid's absolute magnitude needed to be better calibrated. The unusually wide range of phase angles during the observations, ranging from 14.79° to 2.93°, suggested to us that even a value of G might be derived.

The kinetic energy of the impact was independently inferred from the luminosity of the fireball (Borovicka and Charvat 2009) and the infrasound signal (Chesley et al. 2008; Jenniskens et al. 2009). Other measurements of asteroid size came from cosmic ray exposure studies (Welten et al. 2010). It is hoped that all data together will provide an accurate picture of the asteroid's size, mass, and kinetic energy just prior to impact.

The peak-to-peak brightness variations in the lightcurve have also provided information about the shape of the asteroid and its rotation state (Scheirich et al. 2010). Period analysis gave a Fourier period of 49.0338 ± 0.0007 s and 96.987 ± 0.003 s (Jenniskens et al. 2009). A subsequent study showed that the asteroid was in a nonprincipal rotation state (Pravec et al. 2005) with a rotation period $P\psi = 99.19 \pm 0.07$ s and a precession period $P\varphi = 97.00 \pm 0.09$ s (Scheirich et al. 2010).

In this article, a long series of unfiltered CCD images of the asteroid is carefully calibrated to determine the absolute magnitude, H, G, and a crude estimate of the shape, size, and mass of the asteroid, and the results are compared to those derived by other techniques.

INSTRUMENTAL SETUP AND OBSERVING PROCEDURES

After being notified by a colleague about the incoming object around 19 UT on 6 October, photometric data were obtained starting just before the end of astronomical twilight at 23:51 UT and continued until 2008 TC_3 entered Earth's shadow about 2 h later. The Moon (1 day shy of first quarter) was low in the sky and set at 02:45 UT.

Due to the rapid motion across the sky, a script was created to modify the telescope tracking rates every second so that the asteroid image would not be streaked or drift out of the field of view. A Lumenera LW075M USB camera was utilized, which has a 640×480-pixel chip using 7.4 μm pixels in a 4.7×3.6 mm array. Each pixel is capable of recording in 8 bit or 12 bit depth; data were obtained in the 12 bit mode. The camera used an electronic global shutter allowing simultaneous integration of the entire array. The CCD produced an interline transfer progressive-scan image. Images were streamed uncompressed over the USB bus in 16 bit digital form and were stored directly onto a computer.

The camera was installed unfiltered on the Clay Center Observatory's 0.64 m f/9.6 Ritchey-Chrétien telescope, which was focal reduced to f/3.2 to maximize the signal-to-noise ratio of the data, give a wider field of view, and to give as fast of a cadence as possible. This yielded a field of view of $7.0' \times 5.2'$ at an effective focal length of 2,032 mm. Using proprietary image-capturing software, 4 s integrated exposures were taken, which gave an imaging cadence of 4.14 s.

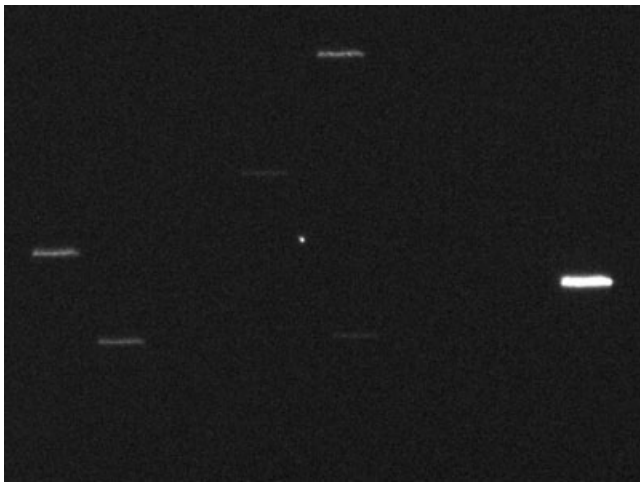

Fig. 1. Frame 1192 showing 2008 TC_3 in the center of the field with a signal-to-noise ratio of 762.

DATA ANALYSIS PROCEDURES

Data were collected from October 6, 2008, 23:48:02.46 UTC to October 7, 2008, 01:48:44.35 UTC, during which 1,770 frames were obtained. The asteroid was imaged until it entered Earth's shadow. Initial entry into the penumbra was detected at 01:47:42 UTC and disappeared below our detection threshold (approximately $V = 16$) at 01:48:37 UTC. The frame from 01:10:00.4 UTC is shown in Fig. 1. From this data, a preliminary instrument lightcurve was obtained by extracting the sum pixel intensity for each asteroid image using the DAOPHOT package.

Our initial absolute magnitude estimate of $H = 30.9 \pm 0.1$ magnitude was obtained by simply detrending this data using a polynomial fit to yield an approximate correction for distance, phase, and extinction effects.

To improve the photometric calibration, these data were reanalyzed using the *xguiphot* IRAF package (Davis 1999), which supports rectangular aperture masks. Because the asteroid was moving rapidly across the sky, up to 7° h^{-1}, the stars were significant trails. A small number of stars pass through the narrow field of view. For each, the x and y positions of the end points of the star streaks were measured, as well as the position of the asteroid in each frame. A rectangular aperture was placed on the midpoint of the star trail and followed in subsequent frames. All stars combined produced a photometric definition file for each frame.

Table 1. Calibration stars and measured magnitudes and color.

Star	Date obs. (2009)	V	$B-V$	$V-R$	$V-M$
TYC 0594-0579-1	9/2	11.597 ± 0.015	1.534 ± 0.031	0.596 ± 0.022	1.872 ± 0.041
TYC 0594-1060-1	9/2	12.538 ± 0.018	0.720 ± 0.032	0.298 ± 0.023	1.688 ± 0.044
TYC 0596-1275-1	9/2	12.550 ± 0.012	0.467 ± 0.024	0.241 ± 0.023	1.652 ± 0.035
TYC 1171-0959-1	9/2	13.096 ± 0.017	1.017 ± 0.039	0.413 ± 0.024	1.746 ± 0.049
TYC 0596-0741-1	9/3	11.359 ± 0.009	0.781 ± 0.015	0.531 ± 0.018	1.821 ± 0.025
TYC 0596-1284-1	9/3	10.363 ± 0.011	0.497 ± 0.016	0.291 ± 0.019	1.708 ± 0.027
TYC 0603-0604-1	9/3	12.421 ± 0.018	0.510 ± 0.028	0.297 ± 0.033	1.683 ± 0.047
TYC 0603-0823-1	9/3	11.983 ± 0.014	0.476 ± 0.021	0.257 ± 0.027	1.668 ± 0.036
TYC 1171-0935-1	9/3	12.022 ± 0.013	0.944 ± 0.022	0.510 ± 0.027	1.086 ± 0.037

Table 2. Landolt fields and RMS residuals for all-sky photometry.

Date	Landolt field 1	Landolt field 2	V_{RMS}	B_{RMS}	R_{RMS}
September 2	F 11	PG0231 + 051 A,B,C,D,E	0.056	0.061	0.050
September 3	PG2331 + 055 A,B	PG2336 + 004 A,B	0.088	0.074	0.119

The asteroid brightness was thus compared to that of the star brightness in each frame. The asteroid brightness was measured using a fixed-sized rectangular aperture. Different-sized aperture masks were used to help adjust for any aperture corrections; however, the photometry proved independent of size of the aperture to a precision of the order of <0.05 magnitude.

As the data were collected using unfiltered light, the color response of the system needs to be calibrated. This was done using all-sky photometry on two photometric nights, September 2 and 3, 2009 using the same camera and telescope setup used for recording the asteroid. *BVR* photometry was done on nine stars visible in the original data set plus some Landolt fields (Landolt 1992) for calibration. Exposures varied from 0.2 to 8.0 s, depending on the brightness of each object through each respective filter. To minimize the effects of scintillation, 25 frames were used for each airmass and filter combination on each target.

All image processing and analysis were performed in IRAF (Tody 1986), with frame calibration accomplished using CCDRED (Valdes 1988), using bias and dark frames. Master dark frames were produced for the CCD frame calibration, with a separate master bias and dark for each night. The all-sky solution was obtained using the DAOPHOT (Stetson 1987) and PHOTCAL (Davis and Gigoux 1993) packages. The results of the all-sky photometry on these nine stars are listed in Table 1. The RMS residuals for the all-sky solution and Landolt fields used for the all-sky photometry are listed in Table 2.

Henden (2000) demonstrated that an unfiltered system could be calibrated to a standard filter within the *UBVRI* system when the system response of the sensor and optical system are known and calibrated. This methodology was adopted by solving the following equation to convert unfiltered instrument magnitude, M, into V instrument magnitude:

$$c_V V + c_B(B-V) + c_R(V-R) + c_0 = M \tag{1}$$

Using Equation 1, we were able to use a least-squares fit to solve for the coefficients, yielding $c_V = +1.0138$, $c_B = -0.0285$, $c_R = -0.4956$, and $c_0 = -1.6925$ with an RMS error of the overall fit of 0.032 magnitude. The Lumenera LW075M response curve is shown in Fig. 2 (Lumenera Corporation 2005).

To get calibrated values from the data, stars were identified by their USNO B1.0 catalog ID using the freeware program C2A by Philippe Deverchère. Each star was then queried in the IRSA Gator Server using their J2000 coordinates. Each star's J and K magnitudes were recorded from the 2MASS catalog (Skrutskie et al. 2006) and transformed using Equation 2 into V, $V-R$, and $B-V$ (Warner 2007) using $V-J$ to calculate V.

$$\begin{aligned} V-J &= 1.4688(J-K)^3 - 2.3250(J-K)^2 \\ &\quad + 3.5143(J-K) + 0.1496 \\ B-V &= 0.2807(J-K)^3 - 0.4535(J-K)^2 \\ &\quad + 1.7006(J-K) + 0.0484 \\ V-R &= 0.3458(J-K)^3 - 0.5401(J-K)^2 \\ &\quad + 1.0038(J-K) + 0.0451 \end{aligned} \tag{2}$$

The extinction coefficient and zero point were determined using a least-squares fit to convert

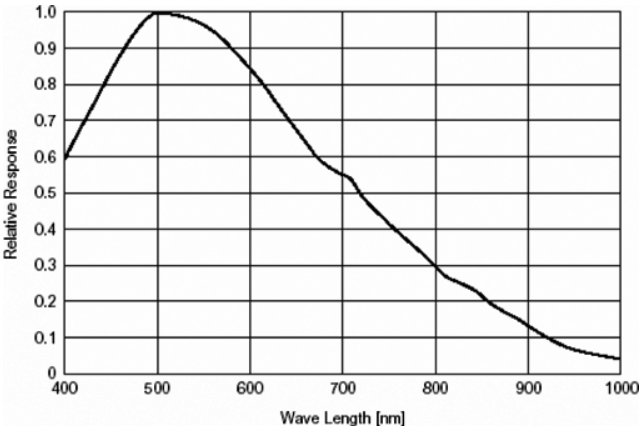

Fig. 2. Spectral response curve of the Lumenera LW075M camera.

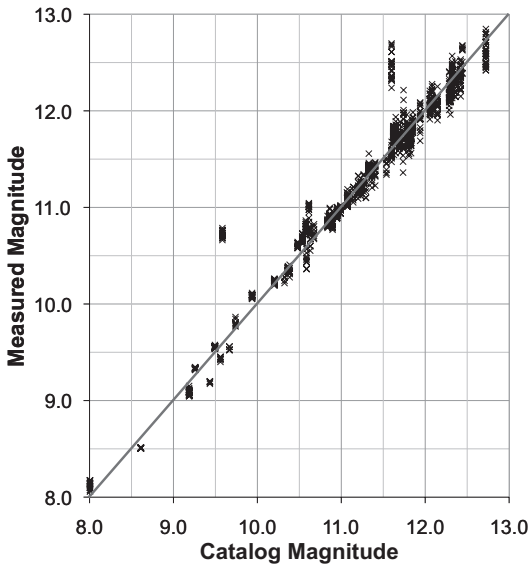

Fig. 3. Photometric fit with the calculated "catalog" unfiltered magnitude on the abscissa and their measured unfiltered magnitude from each frame on the ordinate.

instrument magnitude into unfiltered magnitude using Equation 3, where M is the instrument magnitude, M_0 is the magnitude zero point, K is the extinction coefficient, X is the airmass for that frame, and M_c is the unfiltered calibrated magnitude:

$$M - M_0 - KX = M_c \quad (3)$$

RESULTS

The extinction coefficient was measured over 1.998–1.515 airmasses. Sixty-five stars utilizing 1,015 data points were measured and used to solve the photometry solution. The extinction coefficient was determined to be 0.1065 magnitudes per airmass in unfiltered, and the magnitude zero point was calculated to be 22.14 magnitudes with an RMS error of 0.115 magnitude to the measured stars with scintillation being the dominant source of noise.

The photometric fit of pixel intensities with star magnitudes is shown in Fig. 3. The calculated "catalog" unfiltered magnitude for the calibration stars is shown on the abscissa and their measured unfiltered magnitude from each frame on the ordinate. Four outliers (only two visible on this chart) were excluded from the solution.

The fits obtained from the photometric filter calibration method were better than expected. As the 2MASS catalog has errors in the 0.02–0.03 magnitude range, where $8.5 < K_s < 13$ (Skrutskie et al. 2006), using a large number of stars to solve the all-sky photometric equations can be accomplished with a high statistical accuracy without using typical standard fields.

The largest contribution to noise for the photometric solution in this data set was scintillation due to short exposure times. Variable stars with a large magnitude variation are easily excluded by statistical methods. Assuming a near-photometric night, a data set with a statistically sufficient number of stars and range of airmasses can be calibrated using standard all-sky photometric techniques if standard fields are not available.

The available spectral information of the asteroid and its meteorites were used to calculate the color indexes for the asteroid. The preimpact spectra only covered the wavelength range 554–995 nm (Jenniskens et al. 2009). Fortunately, the spectrum of the meteorite samples is a good match with the preimpact spectra (Hiroi et al. 2010; Jenniskens et al. 2010). From the $B-V$ value of 0.63 ± 0.03 (Hiroi et al. 2010) and a $V-R$ value of 0.35 measured from the spectra of the meteorite fragments (Jenniskens et al. 2010), a calibrated V magnitude was calculated from the unfiltered magnitude of the asteroid in each frame using Equation 1.

The unfiltered, calibrated, but not distance- and phase-corrected lightcurve is shown in Fig. 4. While the asteroid was being imaged it brightened by 2.8 magnitudes in V, almost saturating the CCD near the end. The lightcurve was then corrected for range. The effects of distance are corrected with:

$$V(\alpha) = V_{obs}(\alpha) - 5\log(r\Delta) \quad (4)$$

where r is heliocentric distance and Δ is the geometric distance.

Using the airmass- and range-corrected data, H and G in the system by Bowell et al. (1989) are derived from a least-squares fit of:

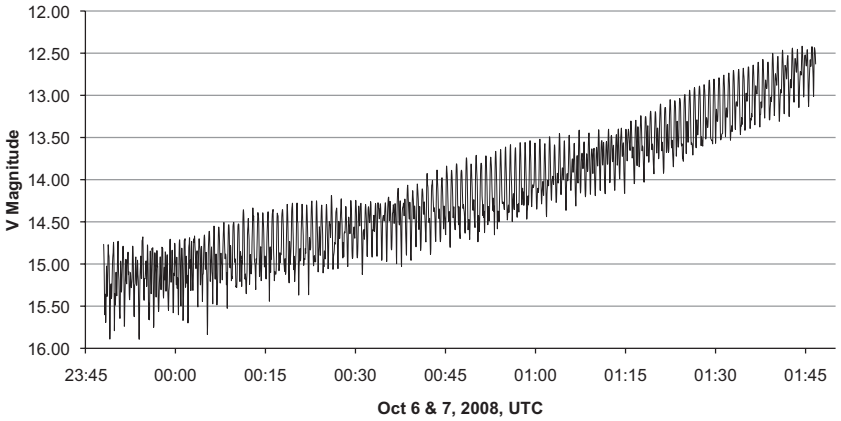

Fig. 4. Unfiltered V-band lightcurve for 2008 TC_3, corrected for atmospheric extinction.

$$10^{-0.4V(\alpha)} = a_1\Phi_1(\alpha) + a_2\Phi_2(\alpha) \tag{5}$$

$$\begin{cases} \Phi_i = W\Phi_{is} + (1-W)\Phi_{iL}; i = 1,2 \\ W = \mathrm{e}^{-90.56\tan^2\frac{1}{2}\alpha} \\ \Phi_{is} = 1 - \dfrac{C_i\sin\alpha}{0.119+1.341\sin\alpha-0.754\sin^2\alpha} \\ \Phi_{iL} = \mathrm{e} - A_i(\tan\frac{1}{2}\alpha)^{B_i} \end{cases} \tag{6}$$

$$A_1 = 3.332 \quad A_2 = 1.862$$
$$B_1 = 0.631 \quad B_2 = 1.218$$
$$C_1 = 0.986 \quad C_2 = 0.238$$

where α is the phase angle and calculating H and G by

$$H = -2.5\log(a_1 + a_2) \tag{7}$$

$$G = \frac{a_2}{a_1 + a_2} \tag{8}$$

The above solution was solved using the Faz program (Bowell et al. 1989). The Faz program was not designed to handle a complex lightcurve like that of 2008 TC_3, but assumes a mean brightness, with rotational variances removed, across the range of phase angles and oftentimes across multiple oppositions. As a result, different selections of data resulted in different values of G, ranging from −0.03 to as high as 0.50.

To improve the value of G and arrive at an accurate value of H, the asteroid shape model was used to remove the periodic oscillations from the lightcurve. Two solutions for the shape model of Scheirich et al. (2010) were used with two different methods to calculate the reflected intensity of light from each model. The first was derived by comparing the intensity reflected by the shape versus the intensity reflected by a sphere at the same geometry. The second was derived by comparing the visible area of the shape versus the visible area of the sphere. The lightcurve calculated from these shape models still had some residuals of about 0.3 magnitude, as the shape model was not a perfect fit to the photometric data.

The four different methods produced values of H = 30.823, 30.818, 30.819, and 30.820 all with an error of ± 0.011 and G = 0.309, 0.297, 0.302, and 0.298 all ±0.014 respectively, using the Faz program.

We then calculated a value for G by plotting a graph of phase on the abscissa and magnitude on the ordinate using Equations 5 and 6, and solved for G using a linear fit to the full data set with a slope of 0. This produced a value of H = 30.86 ± 0.01 and G = 0.33 ± 0.03, consistent with the values produced from the shape model fit.

The final corrected lightcurve, using this value for G, is shown in Fig. 5 with a closeup of part of the lightcurve, to show more detail, in Figs. 6 and 7. $H(\alpha)$ is the absolute magnitude at phase angle α and H is the absolute magnitude at α = 0°.

$$H(\alpha) = H - 2.5\log[(1-G)\Phi_1(\alpha) + G\Phi_2(\alpha)] \tag{9}$$

Using the value obtained for H, the size of the asteroid can be determined based on the currently measured albedos of the recovered fragments. In Table 3 we show the estimated size of 2008 TC_3 using Equation 10 with albedos measured from meteorite fragments of 0.046 ± 0.005 (Jenniskens et al. 2009) and 0.088 ± 0.015 (Hiroi et al. 2010) as there is still uncertainty over which albedo best characterizes this object while it was still in space. The equation for transforming between albedo and the size of the object is given by

$$\log p_{\mathrm{H}} = 6.259 - 2\log d - 0.4H \tag{10}$$

where p_{H} is the albedo, d is the diameter in kilometers, and H is the absolute magnitude (Bowell et al. 1989).

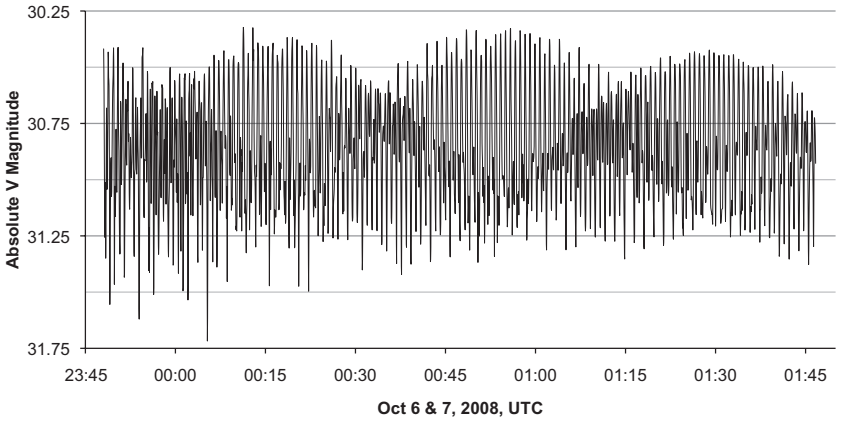

Fig. 5. Unfiltered V-band lightcurve for 2008 TC_3, corrected for atmospheric extinction, range, and phase angle.

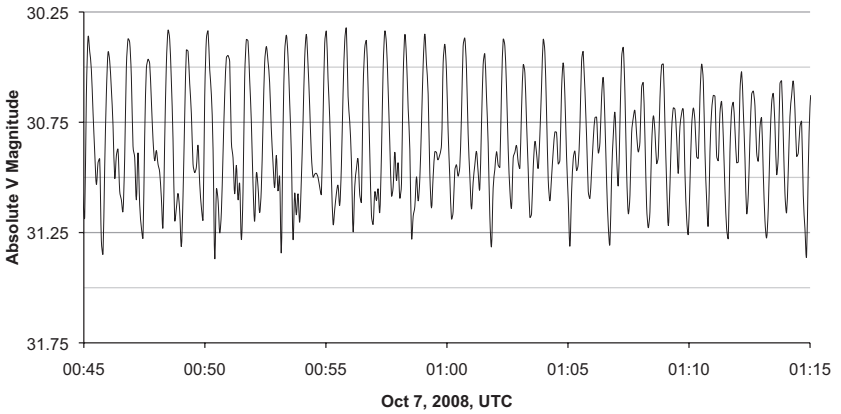

Fig. 6. As Fig. 5, a closeup of part of the lightcurve of 2008 TC_3, covering a 30 min span.

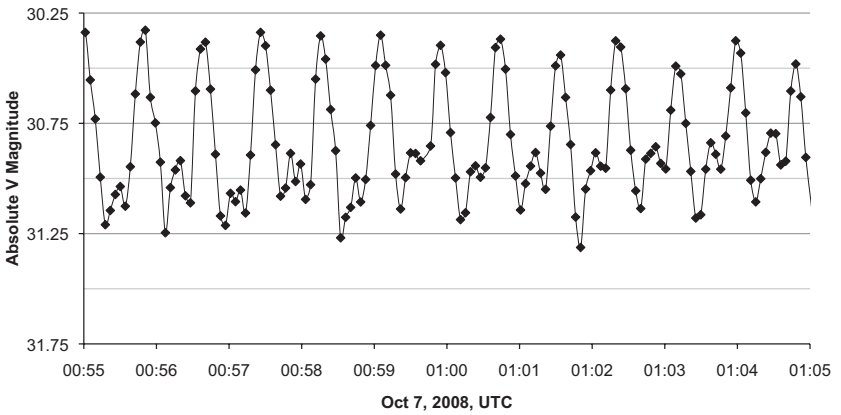

Fig. 7. As Fig. 5, an even more detailed view of the lightcurve, showing data during a 10 min span.

The peak-to-peak variance in brightness was 0.76 magnitude while the RMS variance was 0.27 magnitude and the absolute maximum variation from maximum peak to minimum trough across the entire data set was 1.09 magnitude on the calibrated lightcurve. The variance in brightness of 0.76 magnitude corresponds to almost a 2:1 ratio of the projected area. As the asteroid is in a chaotic rotation state, this ratio is about the

Table 3. Calculated size of 2008 TC_3 in meters and volume in m^3, for mean values of albedo based on the recovered meteorites. The minor and major axes are defined by $H \pm 2\sigma$. Error ranges include albedo and magnitude.

Albedo	Mean diameter	Minor axis	Major axis	Volume
0.046 ± 0.005	$4.25^{+0.30}_{-0.26}$	$3.37^{+0.24}_{-0.21}$	$5.36^{+0.38}_{-0.33}$	$31.80^{+7.32}_{-5.49}$
0.088 ± 0.015	$3.07^{+0.34}_{-0.26}$	$2.43^{+0.27}_{-0.21}$	$3.87^{+0.43}_{-0.33}$	$12.02^{+4.45}_{-2.85}$

Table 4. Table showing volume in m^3, mass in kilograms, and kinetic energy in joules for various albedos and densities. Entries in bold are within the measured range of kinetic energy estimates from luminosity and infrasound signals, whereas entries in bold and italics are those derived from cosmic ray–induced radioactive isotope studies.

		1.0 g cm^{-3}		1.8 g cm^{-3}		2.3 g cm^{-3}		3.1 g cm^{-3}	
Albedo	Volume	Mass	Energy	Mass	Energy	Mass	Energy	Mass	Energy
0.04	39.22	$\mathbf{3.92 \times 10^4}$	$\mathbf{3.20 \times 10^{12}}$	$\mathbf{7.06 \times 10^4}$	$\mathbf{5.77 \times 10^{12}}$	$\mathbf{9.02 \times 10^4}$	$\mathbf{7.37 \times 10^{12}}$	1.22×10^5	9.93×10^{12}
0.05	28.06	2.81×10^4	2.29×10^{12}	$\mathbf{5.05 \times 10^4}$	$\mathbf{4.13 \times 10^{12}}$	$\mathbf{6.45 \times 10^4}$	$\mathbf{5.27 \times 10^{12}}$	$\mathbf{8.70 \times 10^4}$	$\mathbf{7.10 \times 10^{12}}$
0.06	21.35	2.13×10^4	1.74×10^{12}	$\boldsymbol{3.94 \times 10^4}$	$\boldsymbol{3.14 \times 10^{12}}$	$\mathbf{4.91 \times 10^4}$	$\mathbf{4.01 \times 10^{12}}$	$\mathbf{6.62 \times 10^4}$	$\mathbf{5.40 \times 10^{12}}$
0.07	16.94	1.69×10^4	1.38×10^{12}	3.05×10^4	2.49×10^{12}	$\mathbf{3.90 \times 10^4}$	$\mathbf{3.18 \times 10^{12}}$	$\mathbf{5.25 \times 10^4}$	$\mathbf{4.29 \times 10^{12}}$
0.08	13.87	1.39×10^4	1.13×10^{12}	2.50×10^4	2.04×10^{12}	3.19×10^4	2.60×10^{12}	$\mathbf{4.30 \times 10^4}$	$\mathbf{3.51 \times 10^{12}}$
0.10	9.92	9.92×10^3	8.10×10^{11}	1.79×10^4	1.46×10^{12}	$\boldsymbol{2.28 \times 10^4}$	$\boldsymbol{1.86 \times 10^{12}}$	3.08×10^4	2.51×10^{12}
0.12	7.55	7.55×10^3	6.16×10^{11}	1.36×10^4	1.11×10^{12}	1.74×10^4	1.42×10^{12}	2.34×10^4	1.91×10^{12}
0.15	5.40	5.40×10^3	4.41×10^{11}	9.72×10^3	7.94×10^{11}	1.24×10^4	1.01×10^{12}	1.67×10^4	1.37×10^{12}
0.18	4.11	4.11×10^3	3.36×10^{11}	7.40×10^3	6.04×10^{11}	9.45×10^3	7.72×10^{11}	$\boldsymbol{1.27 \times 10^4}$	$\boldsymbol{1.04 \times 10^{12}}$

maximum expected variation for the projected area of a triaxial ellipsoid. The range of possible volumes is also listed in Table 3, assuming an oblate spheroid.

DISCUSSION

The determined value of G is out of range for normal larger asteroids of albedo 0.05–0.15. Generally, G has a small value for low-albedo bodies and a higher value for high-albedo bodies (Bowell et al. 1989). A value of $G = 0.33$, however, would suggest an albedo above the range of 0.05–0.15 values measured from the recovered ureilites (Hiroi et al. 2010). 2008 TC_3 was classified as an F-class asteroid (Jenniskens et al. 2009). Main belt F-class asteroids have albedos around 0.058 ± 0.024 and have G values of 0.12 ± 0.08 (Warner et al. 2009), although higher values of albedo are not uncommon (Jenniskens et al. 2010).

Perhaps G is out of range because 2008 TC_3 is not a normal body. Its superfast rotation and tumbling spin state assured that there was no significant regolith or dust on any part of the surface while in space, which is completely unique among any objects in space for which we have well-observed phase curves.

Indeed, some recovered meteorites, such as sample #27 (Shaddad et al. 2010), had flat-faced millimeter-scale surface features that reflected light well. Our result suggests that this type of material characterized the surface of 2008 TC_3. However, until phase-angle dependent laboratory measurements have been made of the albedo of these materials, this suggestion remains speculative.

From Meteosat 8 luminosity measurements of the meteor, a kinetic energy of 4×10^{12} Joules was derived (Borovicka and Charvat 2009), whereas the infrasound signal detected by the Kenyan infrasonic array I32KE gave a kinetic energy of $6.7 \pm 2.1 \times 10^{12}$ joules (Jenniskens et al. 2009). Cosmic ray-induced radioactive isotope studies showed that 2008 TC_3 had a radius of 300 ± 30 g cm^{-2} (Welten et al. 2010). For densities of 1.8, 2.3, and 3.1 g cm^{-3}, this translates to a diameter of 3.3 ± 0.3, 2.6 ± 0.3, and 1.9 ± 0.2 m, and kinetic energies of $2.9 \pm 0.3 \times 10^{12}$, $1.7 \pm 0.2 \times 10^{12}$, and $9.6 \pm 1.0 \times 10^{11}$ joules, respectively.

From the absolute magnitude H, the asteroid's size, mass, and kinetic energy can be calculated if the albedo and density of the asteroid are known. Table 4 shows the range of possible values for different albedos and densities, covering the full range of meteorite densities measured (Shaddad et al. 2010) as well as a lower value of 1.0 g cm^{-3} in case the original object was more porous than the measured meteorites. Entries in bold are within the measured range of kinetic energy estimates from luminosity and infrasound signals, whereas entries in bold *and* italics are those derived from cosmic ray-induced radioactive isotope studies.

Only for a low asteroid density of approximately 1.8 g cm^{-3} can all observations be brought into agreement, in which case the albedo is 0.05 ± 0.01.

Assuming these values for albedo and density, the total original mass of the asteroid was about 51,000 kg. As the entry velocity is well determined at 12.78 km s^{-1} at 100 km (Jenniskens et al. 2009), the total kinetic energy of the entering body was about 4.1×10^{12} joules in this case.

CONCLUSIONS

The absolute magnitude of 2008 TC_3 was $H = 30.86 \pm 0.01$, whereas the slope parameter was $G = 0.33 \pm 0.03$. This is a significant improvement upon our earlier result of $H = 30.9 \pm 0.1$ (for an assumed $G = 0.15$). The uncertainty in the asteroid's albedo is now the limiting factor in measuring the asteroid's dimensions. Based on constraints from other observations, the most likely density is a low 1.8 g cm^{-3}, from which the albedo is 0.05 ± 0.01. Using this albedo and density, the asteroid would be about 4.1 m in diameter, 28 m^3 in volume, and 51,000 kg in mass.

The physical meaning of the high $G = 0.33 \pm 0.03$ compared with that of typical F-class asteroids remains unclear, which makes any physical interpretation of the best-fit G slope parameter speculative. As more of these small fast rotators are observed, how the value for G applies to the physical characteristics of these objects may become better understood.

Acknowledgments—The authors wish to thank Landon and Lavinia Clay for their continuing generous support for the Clay Center Observatory. Additional resources for this project were provided by Dexter and Southfield Schools, without which the observations and data analysis would not have been possible. The authors acknowledge Alan Fitzsimmons, Arne Henden, Peter Jenniskens, and Carey Rappaport, for their invaluable help and contributions to the data analysis presented in this paper. Thanks to Vanessa Thomas for her review and editing of the initial drafts. This research has made use of the NASA/IPAC Infrared Science Archive, which is operated by the Jet Propulsion Laboratory, California Institute of Technology, under contract with the National Aeronautics and Space Administration. This publication makes use of data products from the Two Micron All Sky Survey, which is a joint project of the University of Massachusetts and the Infrared Processing and Analysis Center/California Institute of Technology, funded by the National Aeronautics and Space Administration and the National Science Foundation. A. W. H. was supported by NASA grant NNX 09AB48G and by National Science Foundation grant AST-0907650.

Editorial Handling—Dr. Dina Prialnik

REFERENCES

Borovička J. and Charvát Z. 2009. Meteosat observation of the atmospheric entry of 2008 TC_3 over Sudan and the associated dust cloud. *Astronomy & Astrophysics* 507:1015–1022.

Bowell E., Hapke B., Domingue D., Lumme K., Peltoniemi J., and Harris A. W. 1989. Application of photometric models to asteroids. In *Asteroids II*, edited by Binzel R. P., Gehrels T., and Matthews M. S. Tucson, AZ: The University of Arizona Press. pp. 524–556.

Chesley S., Chodas P., and Yeomans D. 2008. *NASA/JPL Near-Earth Object Program Office Statement*. http://neo.jpl.nasa.gov/news/2008tc3.html. Accessed November 4, 2008.

Davis L. E. 1999. Xguiphot: A new aperture photometry tool for IRAF. In *Astronomical data analysis software and systems VIII*, edited by Mehringer D. M., Plante R. L., and Roberts D. A. ASP Conference Series 172. Seattle, WA: Astonomical Society of the Pacific. 425 p.

Davis L. E. and Gigoux P. 1993. PHOTCAL: The IRAF photometric calibration package. In *Astronomical data analysis software and systems II*, edited by Hanisch R. J., Brissenden R. J. V., and Barnes J. ASP Conference Series 52. Seattle, WA: Astonomical Society of the Pacific. 479 p.

Henden A. A. 2000. The M67 unfiltered photometry experiment. *Journal of the American Association of Variable Star Observers* 29:35–43.

Hiroi T., Jenniskens P., Bishop J. L., Shatir T. S. M., Kudoda A. M., and Shaddad M. H. 2010. Bidirectional visible-NIR and biconical FT-IR reflectance spectra of Almahata Sitta meteorite samples. *Meteoritics & Planetary Science*, doi: 10.1111/j.1945-5100.2010.01097.x.

Jenniskens P., Shaddad M. H., Numan D., Elsir S., Kudoda A. M., Zolensky M. E., Le L., Robinson G. A., Friedrich J. M., Rumble D., Steele A., Chesley S. R., Fitzsimmons A., Duddy S., Hsieh H. H., Ramsay G., Brown P. G., Edwards W. N., Tagliaferri E., Boslough M. B., Spalding R. E., Dantowitz R., Kozubal M., Pravec P., Borovička J., Charvát Z., Vaubaillon J., Kuiper J., Albers J., Bishop J. L., Mancinelli R. L., Sandford S. A., Milam S. N., Nuevo M., and Worden S. P. 2009. The impact and recovery of asteroid 2008 TC_3. *Nature* 458:485–488.

Jenniskens P., Vaubaillon J., Binzel R. P., Demeo F. E., Nesvorný D., Bottke W. F., Fitzsimmons A., Hiroi T., Marchis F., Bishop J. L., Vernazza P., Zolensky M. E., Herrin J. S., Welten K. C., Meier M. M. M., and Shaddad M. H. 2010. Almahata Sitta (= asteroid 2008 TC_3) and the search for the ureilite parent body. *Meteoritics & Planetary Science*, doi: 10.1111/j.1945-5100.2010.01153.x

Kowalski R. A., Beshore E. C., Boattini A., Garradd G. J., Gibbs A. R., Grauer A. D., Hill R. E., Larson S. M., and McNaught R. H. 2008. In MPEC 2008–T50 1–1 (Minor Planet Center, Smithsonian Astrophysical Observatory, 2008).

Landolt A. U. 1992. UBVRI photometric standard stars in the magnitude range 11.5-16.0 around the celestial equator. *Astronomical Journal* 104:340–371, 436–491.

Lumenera Corporation. 2005. *Lu070 Data Sheet*. http://www.lumenera.com/resources/documents/datasheets/industrial/Lu070-Lu075-datasheet.pdf. Accessed December 21, 2009.

Pravec P., Harris A. W., Scheirich P., Kušnirák P., Šarounová L., Hergenrother C. W., Mottola S., Hicks M. D., Masi G., Krugly Yu. N., Shevchenko V. G., Nolan M. C., Howell E. S., Kaasalainen M., Galád A., Brown P., Degraff D. R., Lambert J. V., Cooney W. R., and Foglia S. 2005. Tumbling asteroids. *Icarus* 173:108–131.

Scheirich P., Ďurech J., Pravec P., Kozubal M., Dantowitz R., Kaasalainen M., Betzler A. S., Beltrame P., Muler G., Birtwhistle P., and Kugel F. 2010. The shape and rotation of asteroid 2008 TC_3. *Meteoritics & Planetary Science*, doi: 10.1111/j.1945-5100.2010.01146.x

Shaddad M., Jenniskens P., Numan D., Kudoda A. M., Elsir S., Riyad I. F., Ali A. E., Alameen M., Alameen N. M., Eid O., Osman A. T., Baker M. I. A., Yousif M., Chesley S. R., Chodas P. W., Albers J., Edwards W. N., Brown P. G., Kuiper J., and Friedrich J. M. 2010. The recovery of asteroid 2008 TC_3. *Meteoritics & Planetary Science*, doi: 10.1111/j.1945-5100.2010.01116.x

Skrutskie M. F., Cutri R. M., Stiening R., Weinberg M. D., Schneider S., Carpenter J. M., Beichman C., Capps R., Chester T., Elias J., Huchra J., Liebert J., Lonsdale C., Monet D. G., Price S., Seitzer P., Jarrett T., Kirkpatrick J. D., Gizis J. E., Howard E., Evans T., Fowler J., Fullmer L., Hurt R., Light R., Kopan E. L., Marsh K. A., McCallon H. L., Tam R., Van Dyk S., and Wheelock S. 2006. The two micron all sky survey (2MASS). *Astronomical Journal* 131:1163–1183.

Stetson Peter B. 1987. DAOPHOT—A computer program for crowded-field stellar photometry. *Publications of the Astronomical Society of the Pacific* 99:191–222.

Tody D. 1986. The IRAF data reduction and analysis system. Instrumentation in astronomy VI. Proceedings of the Meeting, Tucson, AZ, March 4–8, 1986. Part 2 (A87-36376 15-35). Bellingham, Washington: Society of Photo-Optical Instrumentation Engineers. 733 p.

Valdes F. 1988. The IRAF CCD reduction package: CCDRED. Instrumentation for ground-based optical astronomy, present and future. In *The Ninth Santa Cruz Summer Workshop in Astronomy and Astrophysics*, July 13–24, 1987, Lick Observatory, edited by Robinson L. B. New York: Springer-Verlag. LC # QB856. S26 1987. ISBN # 0-387-96730-3. 417 p.

Warner B. D. 2007. Initial results of a dedicated H-G project. The minor planet bulletin (ISSN 1052-8091). *Bulletin of the Minor Planets Section of the Association of Lunar and Planetary Observers* 34:113–119.

Warner B. D., Harris A. W., and Pravec P. 2009. The asteroid lightcurve database. *Icarus* 202:134–146.

Welten K. C., Meier M. M. M., Caffee M. W., Nishiizumi K., Wieler R., Jenniskens P., and Shaddad M. H., 2010. Cosmogenic nuclides in Almahata Sitta ureilites: Cosmic-ray exposure age, preatmospheric mass, and bulk density of asteroid 2008 TC_3. *Meteoritics & Planetary Science*, doi: 10.1111/j.1945-5100.2010.01106.x.

Yeomans D. 2008. *NASA/JPL Near-Earth Object Program Office Statement*. http://neo.jpl.nasa.gov/news/news159.html. Accessed October 6, 2008.